1.D Disk Amplifier Design for the OMEGA Upgrade

The OMEGA Upgrade will use as its final amplifier a disk amplifier with a single 20-cm clear aperture as shown in Fig. 44.19. A single-, rather than a multiple-aperture amplifier such as the multisegmented amplifier (MSA), is chosen in order to permit adjustment of individual amplifier gains for power balance[1] on target. This final amplifier is designed with several unique goals in mind. First, in keeping with LLE's direct-drive mission, it must have superior wave-front and polarization characteristics. Second, because of the anticipated pulse widths in the OMEGA Upgrade, it must be a short-pulse amplifier; that is, it must emphasize gain over efficiency. Third, it must be designed for minimum maintenance over a lifetime in excess of 20,000 shots. A prototype amplifier has been designed that incorporates the best aspects of existing designs[2,3] and, in addition, makes some significant improvements. This article describes that amplifier and its projected performance.

Requirements

The 20-cm amplifier is driven by a 15-cm, four-disk amplifier. In this configuration it is required to produce 855 J in an 800-ps main pulse and, simultaneously, 200 J in a 5-ns foot pulse by use of co-propagation.[4] It must do this with 370-J drive for the main pulse and 85-J drive for the foot pulse. The first photon gain of the amplifier is required to be 3.0. These requirements are calculated by using a simple Frantz-Nodvik[5] model of a saturating amplifier with a saturation fluence of 3.75 J/cm^2. Storage efficiency, while not as important a consideration as gain-per-unit path in glass, should not be less than 1% for cost considerations. Passive losses are specified to give the amplifier a 96% transmission.

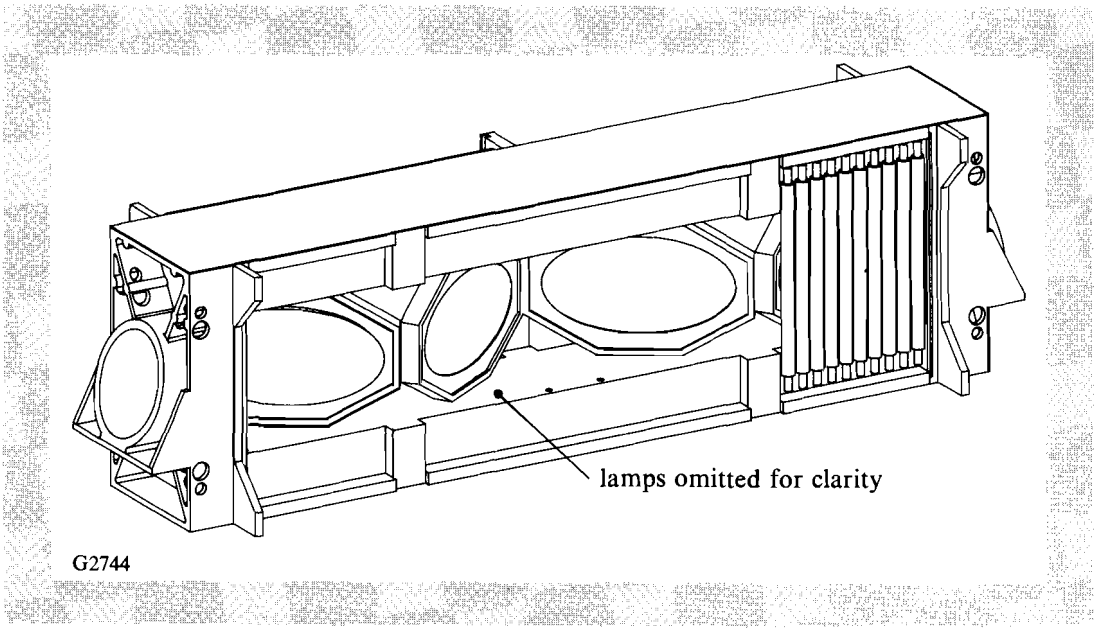

Fig. 44.19
The 20-cm, four-disk amplifier. Note that the transverse flash lamps have been removed for clarity.

The amplifier wave front is expected to be no worse than 0.35 λ rms at 1 μm. In addition to the amplifier wave front at the gain peak (prompt wave front), longer-term (~1-h or steady-state) variations due to post-shot radiative exchange and cumulative shot effects must be minimized in order to meet a one-shot-per-hour repetition rate. Current OMEGA operations are in excess of this rate and the upgrade is planned to be comparable to present OMEGA operations.

Birefringence in the amplifier manifests itself as a spatial beam-intensity modulation and a passive loss both in the amplifier and at the frequency-conversion crystals. The specification of 3.0 nm/cm is driven by the stringent requirement for 3×10^{-4} fractional depolarization at the frequency-conversion crystals. The specification of 3.0 nm/cm is an optimum chosen between what is available at reasonable cost from vendors and the contrast and additional cost of a large-aperture polarizer at the frequency convertors. Birefringence, especially cumulative, also affects the repetition rate.

Finally, although it is difficult to quantify, longevity is a major goal. This, understandably, has its origins in the requirement for high laser availability with low operating costs. There are a number of aspects to amplifier longevity. They include cleanliness, ease of routine service, and solarization resistance. Furthermore, adequate diagnostic capability must be built into the system in order to accurately identify problems should they arise.

Amplifier Description

The amplifier consists of four disks of 3 wt% Nd:phosphate glass, 3.0 cm thick. An even number of disks was chosen in order to obtain adequate gain at the 3.0-cm thickness. The 3.0-cm thickness, 3.0-wt% doping, and 550-μs pump pulse width are optimized for high-gain-per-unit path in glass in order to minimize B-integral. A diagram of a disk is shown in Fig. 44.20. The disk is octagonal with 30° and 60° corners. The disk is clad with 1-μm-absorbing, Cu-doped phosphate glass using a polymer-bonding technique.[6] The thickness of the cladding glass has been increased to 0.8 cm for an absorption-thickness product of 2.8 (3.5-cm^{-1} absorption). Distributing the amplified spontaneous emission (ASE) energy over a greater thickness reduces the peak cladding temperature rise during a shot, thereby reducing the stress on the bond to the laser glass and the deformation induced in the laser glass by the expanding cladding.[7] Superimposed on the disk in Fig. 44.20 is the elliptical projection of the clear aperture. In the LLE design, additional laser glass (2.5 cm) has been left between the top and bottom edge of the clear aperture and the cladding in order to remove the area of greatest beam steering from the clear aperture.

The laser disk is held in a disk frame (Fig. 44.21) that is an octagonal ring of 6061-T6 aluminum, the same depth as the minimum disk thickness. The disk rests directly on the bottom inside of the ring. One side of the ring has a lip that forms the disk mask on one side of the disk. A disk mask is attached

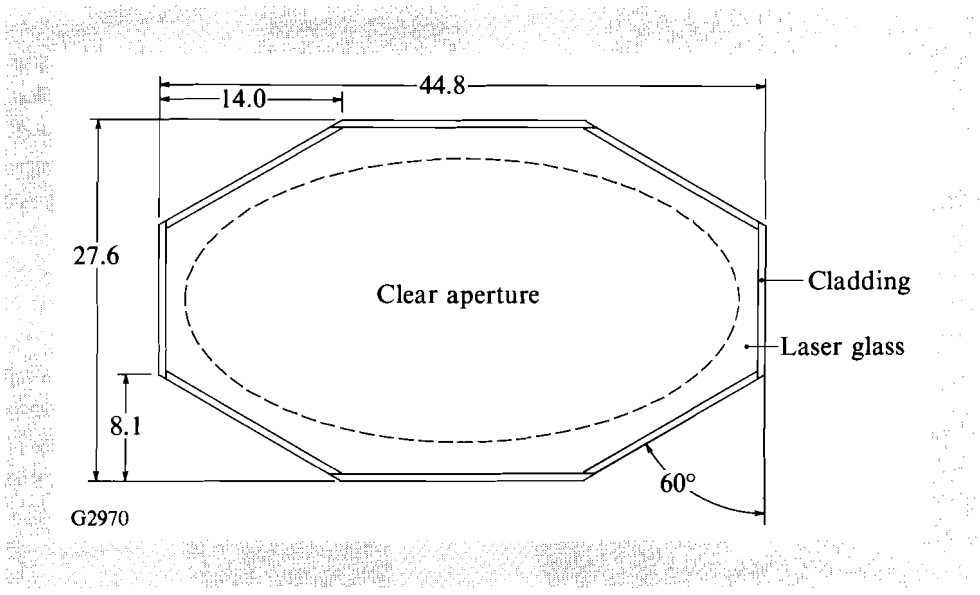

Fig. 44.20
The clad 20-cm laser disk. The location of the clear aperture is marked by the ellipse on the disk face.

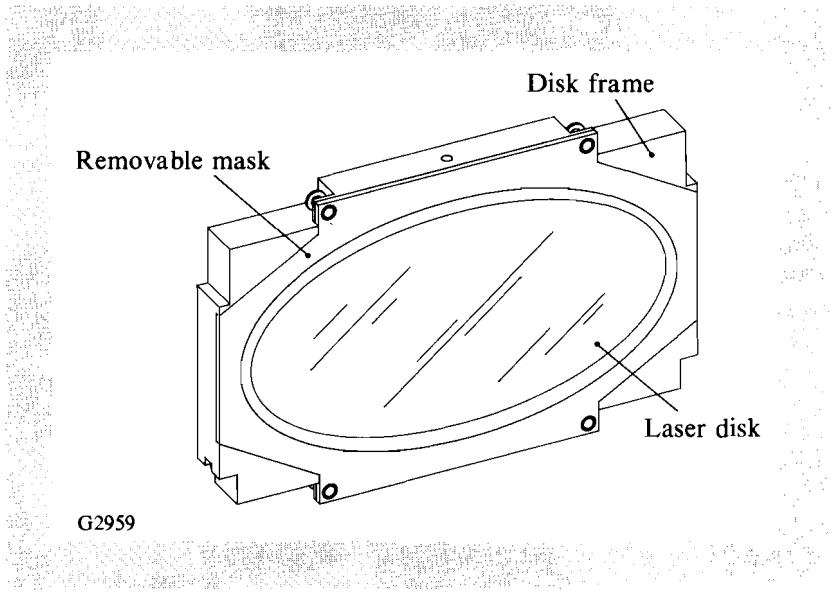

Fig. 44.21
The disk frame. The disk frame supports the disk and shields the cladding and extra laser glass from flash-lamp light.

to the opposite side of the ring with four clevis-pin-held springs.[8] The force exerted by the removable mask just equals the weight of the disk. Side-to-side motion of the disk is prevented by marcel springs. The complete spring loading of the disk insulates it from any mounting-induced deformations; in essence, the disk defines its own plane. To further alleviate any potential mounting deformations, the disk frame is mounted into the amplifier frame using a three-point kinematic mount.

The amplifier frame is a four-part casting consisting of top, bottom, and end plates. End plates are pinned and bolted to the top and bottom plates.

The material is aluminum for lightness and ease of manufacturing. Stiffening ribs have been strategically located to reduce part bending and frame "torquing." Vertical members connect the top and bottom plates at locations along the side of the amplifier where disk frame edges meet. V-groove blocks that support the disk frames bolt to the verticals. By separating the frame into four pieces acceptable rigidity is obtained with greatly improved ease of cleaning, assembly, and manufacturing. Disk frame assemblies containing the glass disks are easily loaded into the amplifier frame from the sides. The top and bottom frame members are covered by curved sheet-metal reflectors that are convex into the amplifier volume. Purge gas (clean N_2 or clean air) is introduced into the amplifier cavity behind the upper reflector. Protective blast windows mount to the sides of the amplifier frame. These windows reflect the acoustic wave generated by firing the flash-lamp arrays and isolate the clean interior of the amplifier.

Pump modules (Fig. 44.22) containing the flash lamps and their reflectors attach to the sides of the amplifier over the blast windows. Pump modules are either short or long types depending on whether a module pumps one or two disks. The modules are designed to unlatch and tilt away from the amplifier for *in-situ* replacement of failed flash lamps. (The amplifier stays in place while a lamp module is replaced.) A long module

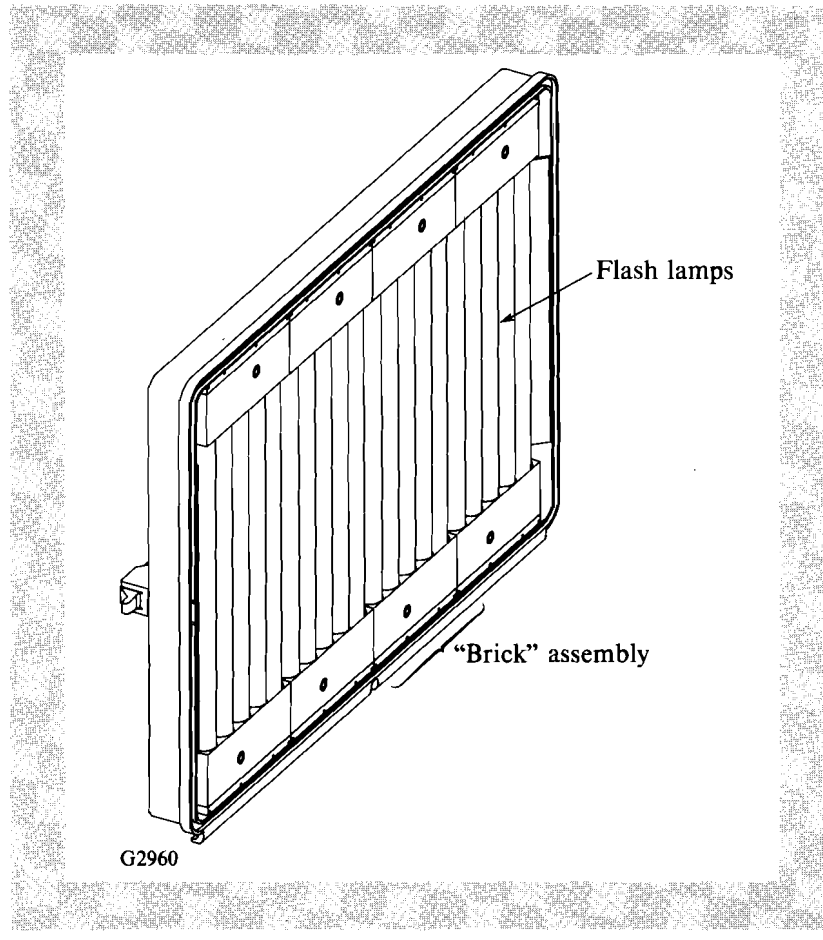

Fig. 44.22
The long-pump module. The long-pump module contains four brick assemblies of five flash lamps each. A simple flat reflector is behind the bricks. The pump module is purged with N_2. The short-pump module is similar but contains only 10 lamps.

contains 20 lamps and a short module contains 10, for a total of 80 transverse-mounted lamps in the amplifier. The lamps are mounted on 1.341-in. centers. Five lamps are connected in series to make a brick. One pulse-forming network (PFN) drives one brick. The individual lamps are 1.9-cm bore with a 10-in. arc length. The lamps are water cooled and cooling is series connected within a brick. A brick is the smallest serviceable component on the in-system amplifier. New brick assemblies are built up off-line in a clean room and are readily installed into amplifiers that may be as high as 3.5 m above the laser bay floor. Simple flat reflectors are used in the pump module because of the close spacing of the water-jacketed lamps.

Water cooling of flash lamps has been retrofitted into existing disk amplifiers at other laboratories.[9] Water cooling has been specified in this amplifier for a number of reasons. First, it virtually eliminates catastrophic lamp failures without having to test every lamp for infant mortality. Second, it allows the use of much-lower-cost lamp-seal technologies such as solder-seal or hard-seal lamps instead of reentrant- or reverse-reentrant-seal lamps. Third, it eliminates the post-shot thermal-soak problem where heat from the lamp walls is radiatively transported to the laser disks causing additional disk deformation. Fourth, in high-voltage systems, deionized water is an excellent insulator, eliminating corona and flashover problems.[10] Deionized water has also been successfully used on the rod-geometry amplifiers in the current OMEGA laser system.

Transverse mounting permits locating the lamps much closer to the disks than is possible with longitudinal lamps. This is especially true since the disks have extra glass and concomitant larger holders in order to keep cladding-induced disk deformations out of the clear aperture. Ray-tracing calculations indicate that the improvement in a new (i.e., untarnished reflectors) amplifier is ~4% in stored energy density for transverse versus longitudinal lamps. The difference between transverse and longitudinal efficiencies can be expected to increase with amplifier age. The transverse mounting with its compact $8 \times 21 \times 2$-in. flash-lamp brick is also vastly more serviceable than the 1×65-in. glass and quartz assemblies that would be required for the longitudinal case. Furthermore, the vertical mounting of the lamps avoids the horizontal, longitudinal case tendency of the water jacket to sink and the flash lamp to float.

Each flash-lamp brick is driven by a single-mesh L-C circuit of 210 μF and 160 μH. Nominal charging voltage is 14.1 kV. The same pulse-forming networks will be used for the 15-cm disk amplifier. The lamps will be triggered by "ringing up" the lamp-cable capacitance. The PFN's are individually equipped with current monitors so that misfiring bricks may be readily identified. In addition to the main discharge, all lamps will be preionized[11] 100–200 μs prior to the initiation of the main discharge in order to increase Nd^{+3}-pumping efficiency, reduce hard-UV emission, and reduce lamp-wall stresses.

Calculated Amplifier Performance

Calculations made to estimate amplifier performance have concentrated on beam-quality issues associated with the amplifier: gain uniformity, beam steering, focusing, etc. Gain uniformity and disk deformation require a knowledge of the spatial distribution of either heat or inversion throughout the amplifier. Monte-Carlo pump-light ray tracing[12,13] has provided a useful tool to determine the spatial distribution of inversion. Using the proportionality constant χ,[14] the deposited heat may also be estimated.

Symmetry in the amplifier can be used to reduce the ray-tracing problem to only one quadrant of the amplifier. Two million rays at 200 wavelengths are traced in a typical single-quadrant calculation. *S* and *P* average polarization properties are used. Arbitrary reflection/refraction properties may be assigned to surfaces. Similarly, arbitrary absorption/emission characteristics may be assigned to any volume. The capability to model spectral shifts is important in estimating aging effects where materials solarize, reflectors tarnish, etc.

The ray-tracing results show that the two interior disks are much more uniformly pumped than the two end disks. This is shown in Figs. 44.23(a) and 44.23(b). The plot is of average relative stored-energy density for each cm of the 3-cm disk thickness. The large variation across the disk thickness is of little importance because the beam propagates across this gradient. The variation along the disk major axis is, however, critical. This determines the gain uniformity across the clear aperture of the amplifier and the disk bending. The two innermost (interior) disks are uniformly pumped across the major axis to within the error bars of the code ±8%. The majority of the gain variation and disk bending comes from the two end (exterior) disks, which exhibit a 40% variation across their exterior sides. The thickness-averaged stored-energy density is more uniform resulting in less aperture variation.

The normalized, calculated, small-signal gain profile for the amplifier is shown in Fig. 44.24. The 15% variation from side to side in the horizontal direction is typical of disk amplifiers with an even number of disks.[15] The gain variation in the vertical direction is typically at least a factor of 3 smaller. The horizontal gain variation can be significantly flattened by orienting the 15-cm-driver disk amplifier to have its "hot" side in series with the 20-cm cold side. The resultant stage small-signal gain profile is shown in Fig. 44.25.

Since the deposited heat is, to first order, proportional to the stored-energy density, the calculated stored-energy profile may be used as input to a model of the disk surface displacement. A two-dimensional model of the disk cross section on the major axis was constructed. The deposited heat was assumed to be identically zero outside of the disk clear aperture. This model used the plane-strain approximation wherein the disk is assumed to be infinite in the vertical direction. Spring-support boundary conditions were used on the disk edges in simulation to model the actual disk mounting

as accurately as possible. The biharmonic equation[16] was then solved for the Airy stress potential[17] via a finite-element method. Linear elastic-constitutive relations of the glass are used to obtain the displacement field. The solution was checked to ensure that the boundary conditions were satisfied.

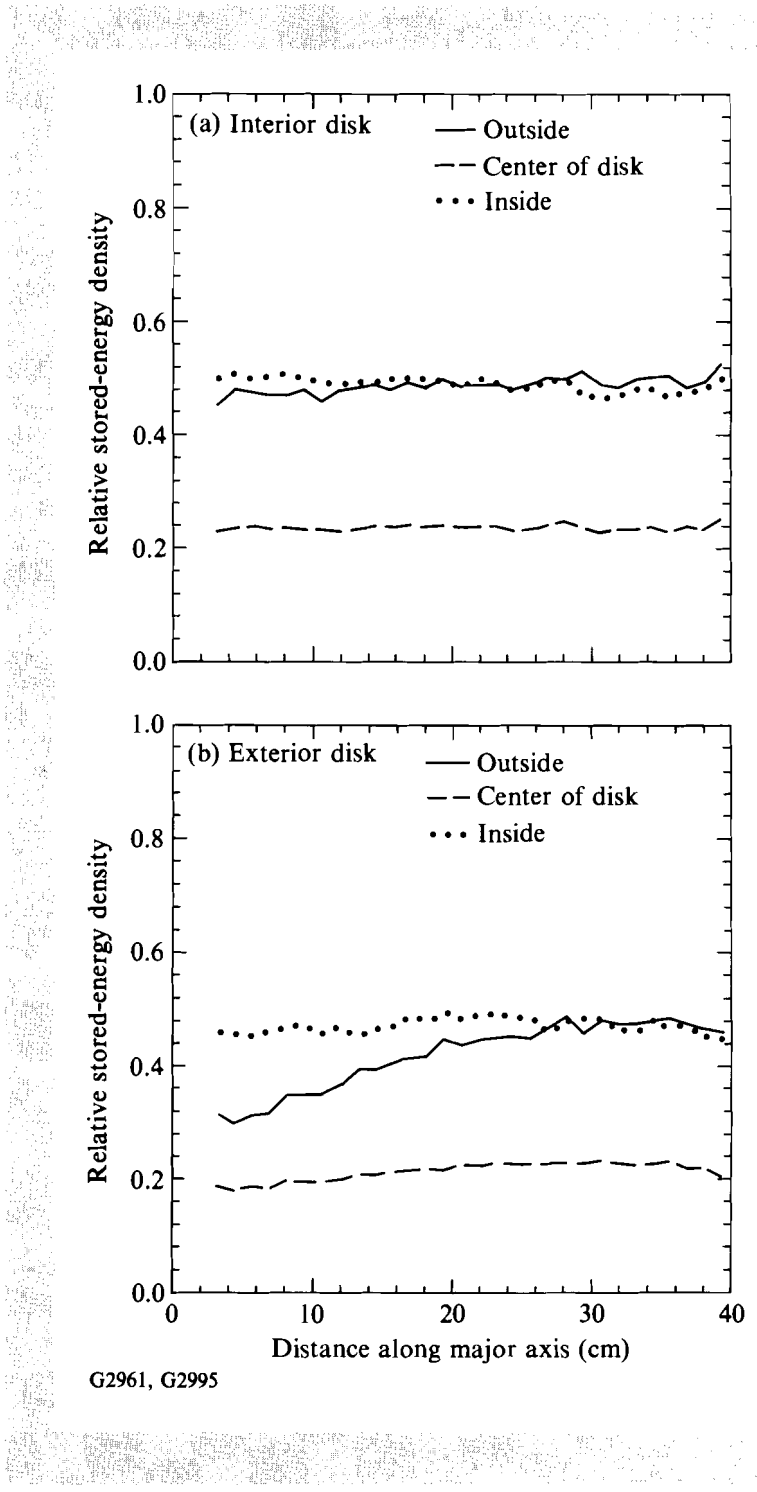

Fig. 44.23
Calculated relative stored-energy density along the major axis of the interior (a) and exterior (b) disks. Variation along the major axis affects disk bending and gain uniformity. The large variation across the disk thickness is unimportant. The interior disk is uniform to within ±8% along the major axis. The change along the major axis of the exterior disk will account for nearly all of the amplifier's gain asymmetry and wave front.

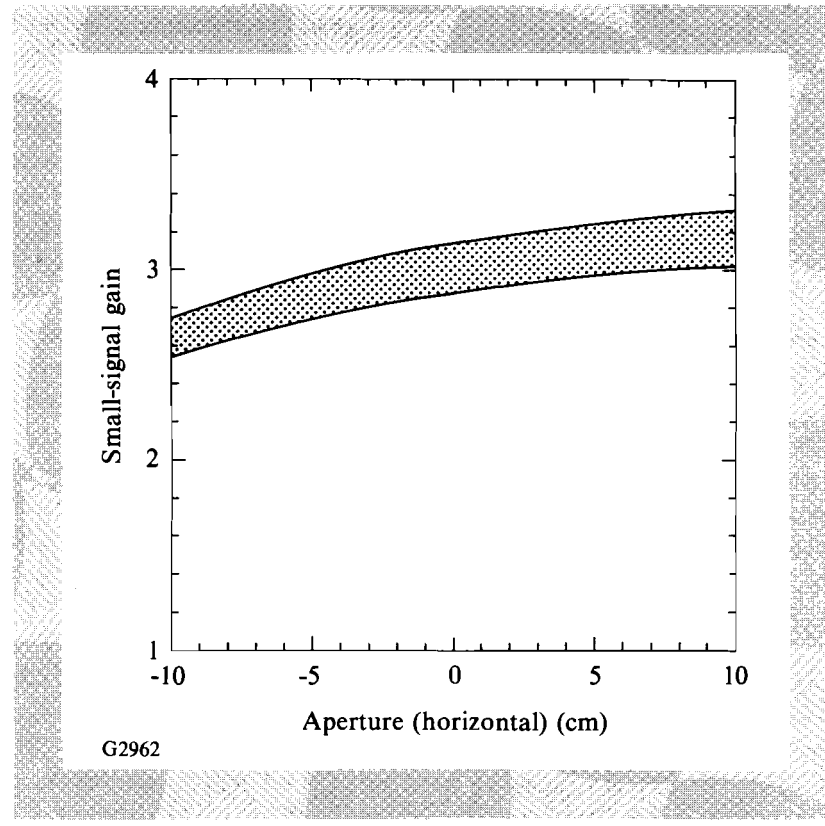

Fig. 44.24
Calculated small-signal gain of the 20-cm amplifier versus aperture.

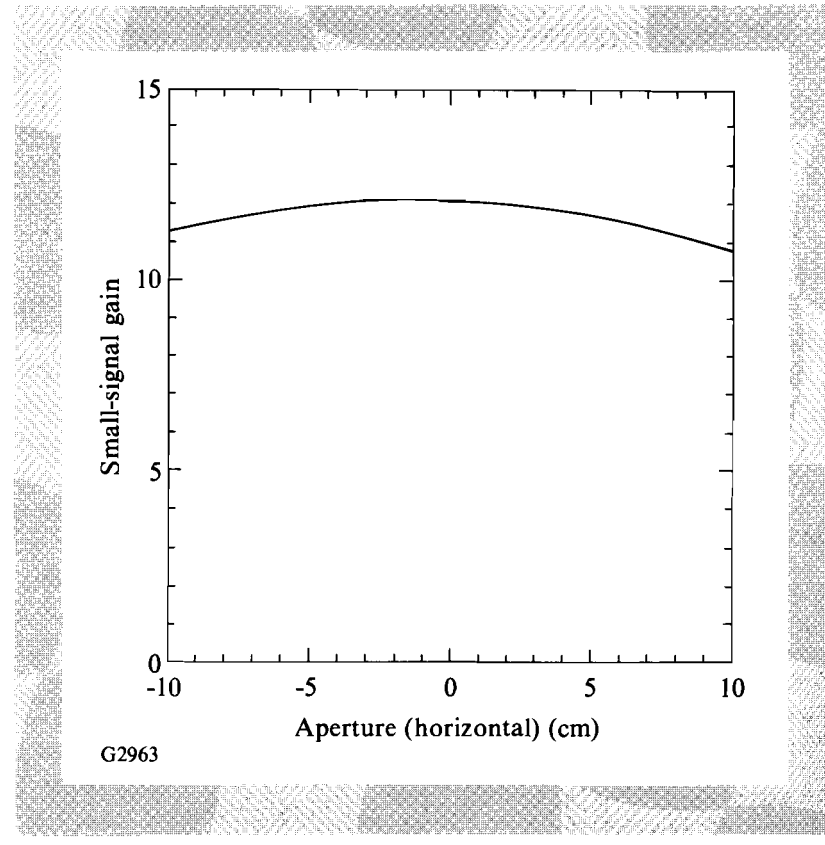

Fig. 44.25
Calculated combined small-signal gain of the 15- and 20-cm amplifiers. The resultant gain is uniform to within ±7%.

If the displacements of the two surfaces are nearly parallel the effect is a bending of the disk (excepting the trivial case of a uniform expansion of the disk). The sensitivity to bending is greatly increased because the disk is at Brewster's angle (see Fig. 44.26). A bending of the disk in the plane of incidence to a constant radius of curvature causes a whole-beam steering. Any variations in the radius of curvature cause higher-order aberrations. These conclusions assume that the coefficient of optical path for the glass is small ($<1.0 \times 10^{-6}$ °C) and that stress-optic effects are negligible. The beam steering δ is given by[18]

$$\delta = \frac{n^2 - 1}{n} \frac{t}{R},$$

where n is the refractive index, t is the disk thickness, and R is the radius of curvature of the bent disk.

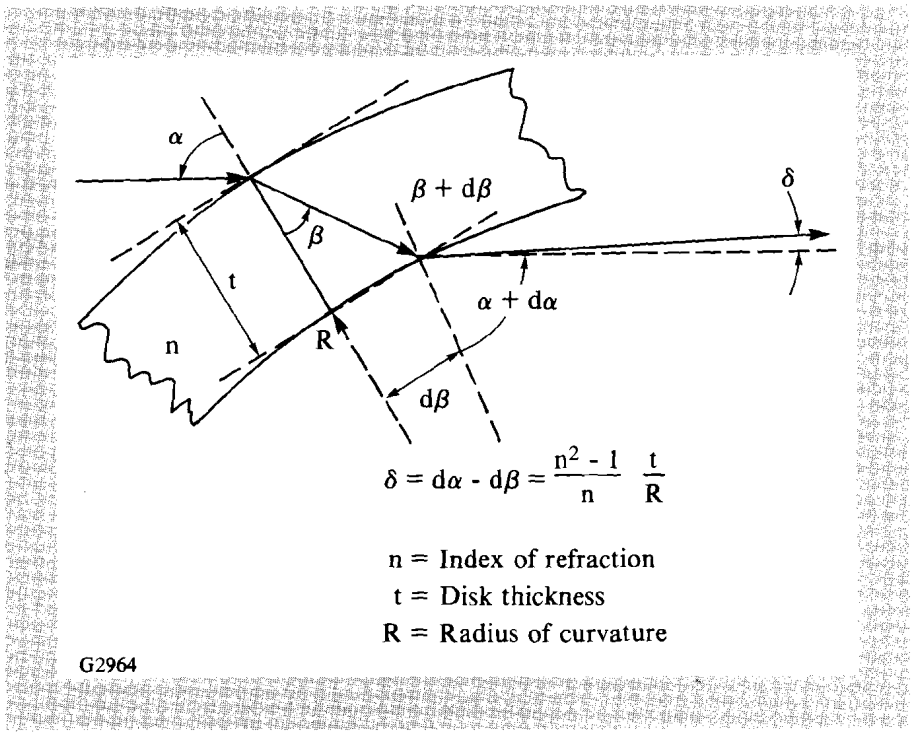

Fig. 44.26
Beam steering due to disk bending.

A plot of surface displacements for the end disks is shown in Fig. 44.27. For this set of conditions the disk displacements are small (~1 μm) and the disk bends with the concave surface out (toward the end of the amplifier). The associated wave front for the amplifier is shown in Fig. 44.28 and is seen to consist of primarily a beam steering in the horizontal plane (~2.5 μrad) and a very weak astigmatism. Note that these results were obtained with a two-dimensional model. Work is continuing on a three-dimensional model to determine the surface displacements along the vertical direction.

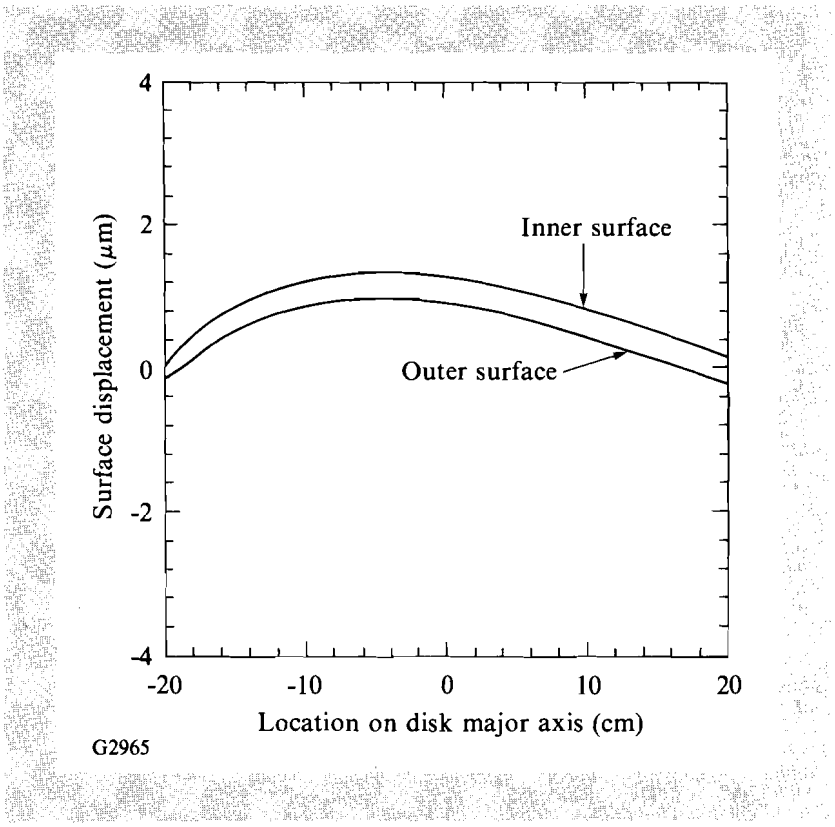

Fig. 44.27
Surface displacement in microns versus aperture in the horizontal direction. The outside of the amplifier is down in this diagram.

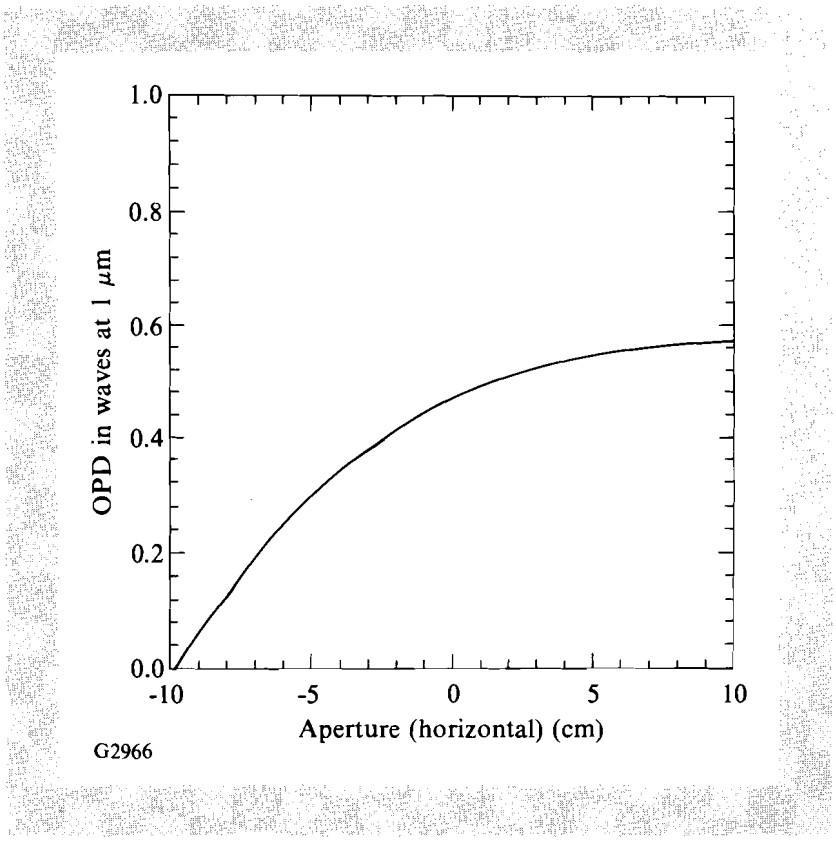

Fig. 44.28
The calculated wave front in the horizontal direction due to prompt disk bending. The beam propagates up in this diagram. The wave front consists primarily of a pointing change and an astigmatic component.

Beam steering due to ASE heating of the cladding glass is not anticipated to be a problem during a shot. The results of a calculation of the surface displacement induced by the cladding expansion is shown in Fig. 44.29. The previously described extra 2.5 cm of laser glass removes the distorted region from the clear aperture. Further calculations are underway to assess the heat removal from the cladding region through the disk masks.

The prompt thermally induced bending of the disks is not the only contributor to the wave-front error of the amplifier. Disk-finishing errors, acoustic effects, etc., also occur. One realization of the passive wave front of the amplifier due to finishing errors is shown in Fig. 44.30 where the interferometrically measured[19] passive wave fronts of four of the MSA disks were added to estimate the passive wave front of the single-segmented amplifier (SSA). The MSA disks are slightly thicker (3.3 cm versus 3.0 cm) and slightly larger (24-cm versus 20-cm clear aperture). Therefore, the resultant summation will be a slightly conservative estimate of the passive wave front. The wave-front rolloff near the edge in the horizontal direction is characteristic of polishing finite plates. The peak-to-valley wave front is ~0.25 λ at 1 μm, substantially below the specification for total wave front (both active and passive).

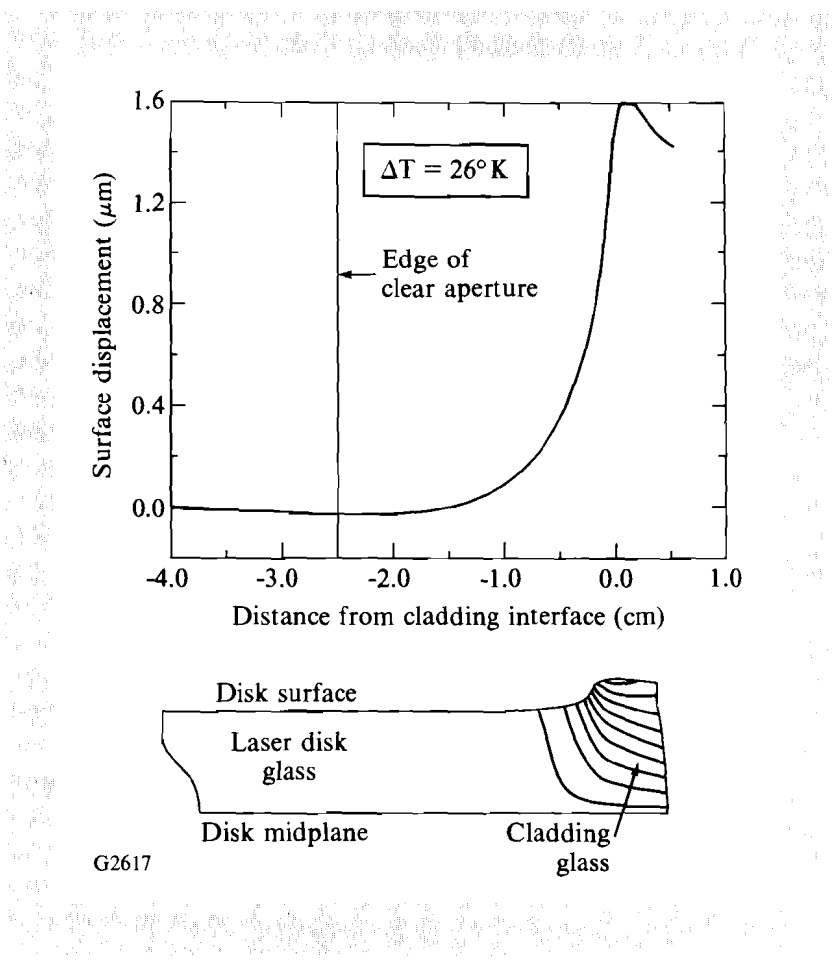

Fig. 44.29
The calculated surface displacement due to heated cladding. The edge of the clear aperture, indicated in the diagram, is well removed from the region of greatest steering.

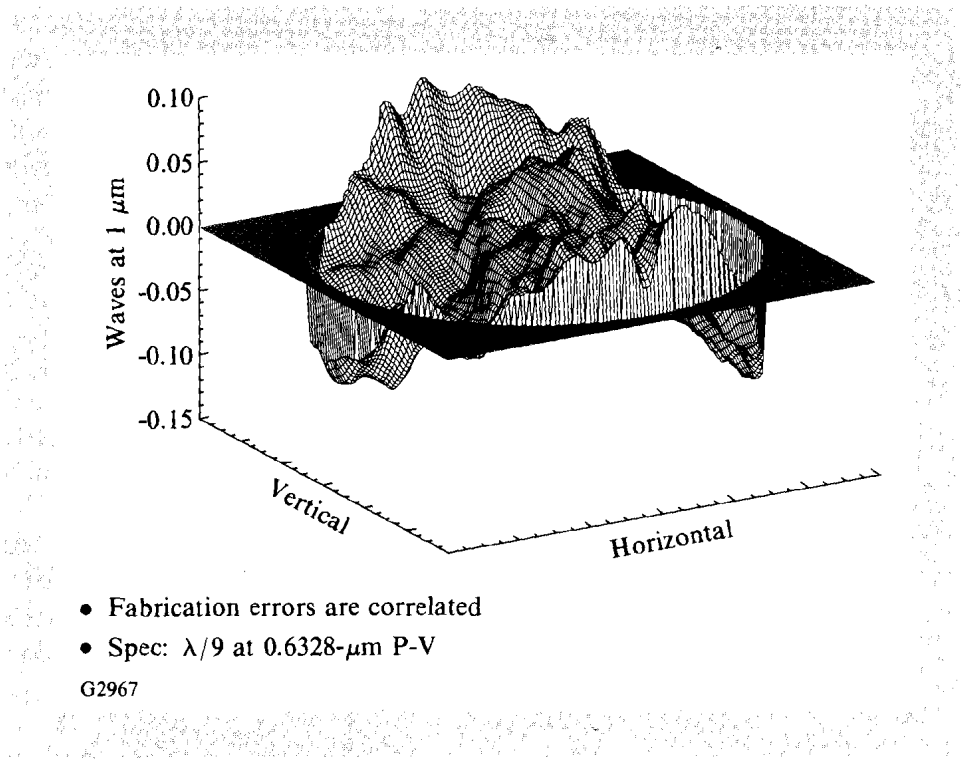

Fig. 44.30
Interferometrically measured wave front of four multisegmented amplifier (MSA) disks in series. Although these disks are slightly larger and slightly thicker than the 20-cm amplifier disks, they are indicative of what can be expected from the passive 20-cm amplifier.

The use of Pyrex®[20] water jackets on the cerium-doped quartz flash lamps initially offered the opportunity to eliminate blast windows, thereby reducing costs. It was hypothesized that the Pyrex® UV-absorption edge, which covered the UV window in the cerium-doped quartz absorption at ~250 nm, would eliminate any UV light in the amplifier that molecular oxygen might absorb. Time-resolved interferometric measurements of the atmosphere above a flash-lamp array operated at the equivalent-energy level of the SSA revealed the existence of significant optical-path disturbances as shown in Fig. 44.31. Replacement of the atmosphere with pure N_2 did not affect the result. It is currently hypothesized that these disturbances are due to simple acoustic waves rather than UV absorption. This hypothesis is supported by the significant reduction of the effect when a blast window is reintroduced as shown in Fig. 44.32. The blast window should act as an acoustic-impedance mismatch, keeping most of the acoustic energy in the pump module. As a result of these measurements, the 20- and 15-cm disk amplifiers used on the OMEGA Upgrade will have blast windows.

Conclusion

The OMEGA Upgrade will use a 20-cm, single-aperture disk amplifier as the final amplifier. In keeping with LLE's direct-drive mission, special emphasis has been placed on understanding the amplifier's gain uniformity and wave-front quality before actual construction of hardware. Construction of the prototype amplifier will take place in the last quarter of 1990. Testing of the prototype will begin in the first quarter of 1991. Results of the testing will be reported in a future LLE Review article.

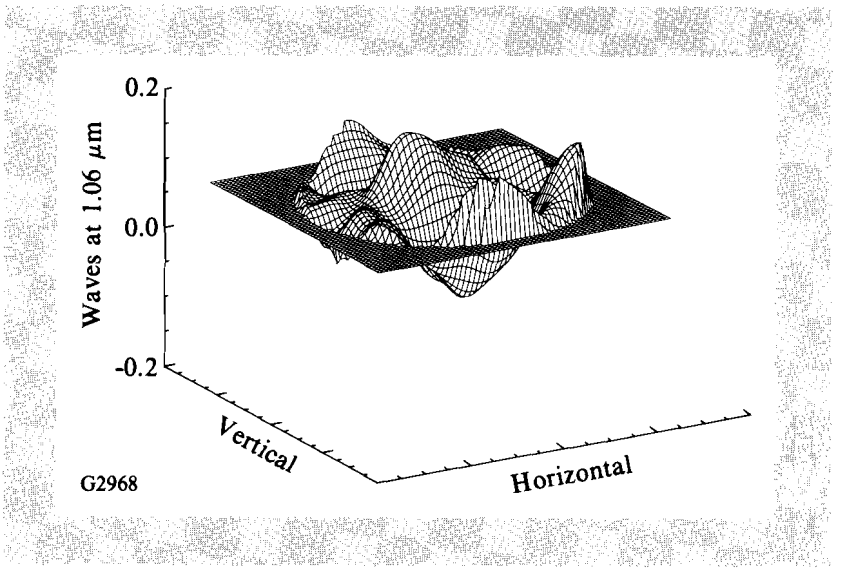

Fig. 44.31
The measured wave front above a 30-cm section of a flash-lamp array without a blast window. The bottom of the beam (closest to the array) is in the foreground.

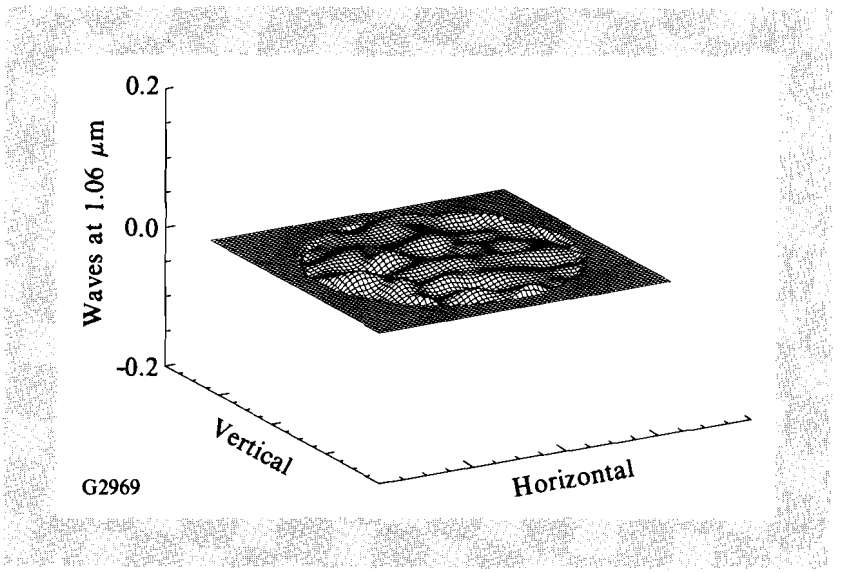

Fig. 44.32
The measured wave front above a 30-cm section of a flash-lamp array with a blast window. The bottom of the beam (closest to the array) is again in the foreground. The remaining wave front is comparable to that of the empty interferometer.

ACKNOWLEDGMENT

This work was supported by the U.S. Department of Energy Division of Inertial Fusion under agreement No. DE-FC03-85DP40200.

REFERENCES

1. LLE Review **41**, 4 (1989).
2. Laser Program Annual Report 1980, Lawrence Livermore National Laboratory, UCRL 50021-80 (1981), pp. 2-234–2-237.
3. Annual Report to the Laser Facility Committee (1985), Rutherford Appleton Laboratory, pp. A6.6–A6.12.

4. OMEGA Upgrade Preliminary Design Document, DOE/DP40200-101 (1989).

5. L. M. Frantz and J. S. Nodvik, *J. Appl. Phys.* **34,** 2346 (1963).

6. Laser Program Annual Report 1986, Lawrence Livermore National Laboratory, UCRL 50021-86 (1987), pp. 4-14–4-56.

7. Laser Program Annual Report 1987, Lawrence Livermore National Laboratory, UCRL 50021-87 (1989), pp. 3-48–3-88.

8. Laser Program Annual Report 1986, Lawrence Livermore National Laboratory, UCRL 50021-86 (1987), pp. 4-55–4-56.

9. Private communication with K. Moncur, KMS Fusion, Inc. (1989).

10. M. Zahn *et al.*, "Dielectric Properties of Water and Water/Ethylene Glycol Mixtures for Use in Pulsed Power System Design," in *Proceedings of the IEEE*, Vol. 74, No. 9 (1986).

11. Laser Program Annual Report 1985, Lawrence Livermore National Laboratory, UCRL 50021-85 (1986), pp. 7-18–7-25.

12. Laser Program Annual Report 1986, Lawrence Livermore National Laboratory, UCRL 50021-86 (1987), pp. 7-142–7-146.

13. The code used is a greatly updated and enhanced version of the code ZAP originally written by Systems, Science and Software for the Naval Research Lab by J. H. Alexander, M. Troost, and J. E. Welch, ARPA order number 660, Contract number N00014-70-C-0341 (1971).

14. M. S. Mangir and D. A. Rockwell, *IEEE J. Quantum Electron.* **QE-22,** 574 (1986).

15. J. E. Murray, H. T. Powell, and B. W. Woods, UCRL-93321 (1986), p. 13.

16. J. Eggleston, Ph.D. thesis, Stanford University, 1982, pp. 16–17. Available from University Microfilms Inc., Ann Arbor, MI.

17. B. A. Boley and J. H. Weiner, *The Theory of Thermal Stresses* (Wiley, New York, 1960), pp. 109–116.

18. Laser Program Annual Report 1982, Lawrence Livermore National Laboratory, UCRL 50021-82 (1983), p. 7–74.

19. Interferometric data supplied by D. Pileri of the Special Optics Fabrication Group, Eastman Kodak Co., Rochester, NY.

20. Pyrex® is a product of Corning Glass Works, Corning, NY.